Deep–Sea Research II 213 (2024) 105354

Contents lists available at ScienceDirect

Deep-Sea Research Part II

journal homepage: www.elsevier.com/locate/dsr2

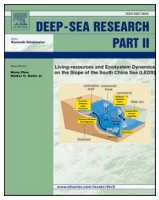

Investigation of ocean environmental variables and their variations associated with major Loop Current eddy-shedding events in the Gulf of Mexico

Nazanin Chaichitehrani *, Ruoying He

Department of Marine, Earth, and Atmospheric Sciences, North Carolina State University, Raleigh, NC, USA

ARTICLE INFO

Handling Editor: Dr. K Drinkwater

Keywords:
Eddies
Loop current
Eddy kinetic energy
Baroclinic instability
Barotropic instability

ABSTRACT

The eddy kinetic energy (EKE) variability associated with 26 major Loop Current eddies (LCEs) in the Gulf of Mexico from 1994 through 2019 was investigated. We employed 3D multivariate observation-based ARMOR3D monthly ocean analyses of salinity, temperature, and geostrophic velocity field data. In addition, we used ERA5 wind data, the fifth generation of the European Centre for Medium-Range Weather Forecasts (ECMWF) atmospheric global climate reanalysis, to analyze internal and external forcing processes affecting the evolution of these LCEs. The energy analysis was performed to understand the role of barotropic (BT) and baroclinic (BC) instabilities and their associated energy conversion mechanisms in EKE generation. Our results suggest that BT instabilities are the primary source of EKE variability in the upper water column of the LC system. Furthermore, BT was positively correlated with Yucatan Channel (YC) transport during these major LCE shedding events. YC transport plays a significant role in energy conversion from mean kinetic energy to EKE, Loop Current growth, and generation of LCEs. BC instability was inversely correlated with buoyancy frequency, and a decrease in stratification triggers the development of BC instability, which favors eddy shedding. An eddy shedding index (ESI) was developed to quantify EKE evolution. Major LCE shedding occurs when ESI $\geq$0.46.

1. Introduction

The Loop Current (LC) is recognized as a highly nonlinear and complex ocean current system that enters the Gulf of Mexico (GoM) through the Yucatan Channel (YC) and exits through the Straits of Florida (SoF) (e.g. Reid, 1972; Hurlburt and Thompson, 1980; Hamilton, 1990; Fratantoni et al., 1998; Oey et al., 2005; Hirschi et al., 2019). The LC plays an essential role in forming the western boundary current in the North Atlantic Ocean (i.e. the Gulf Stream) (Oey et al., 2005). The typical LC cycle involves LC intrusion into the GoM, irregular expansion northward, shedding of anticyclonic warm-core eddies (diameters 200–400 km and lasting 0.5–18 months), and retraction to the port-to-port (YC to SoF) route (e.g. Sturges and Leben, 2000; Leben, 2005; Alvera-Azcárate et al., 2009; Chang and Oey, 2011; Weisberg and Liu, 2017). The LC and LC eddies (LCEs) are the main features of circulation in the GoM, significantly influencing hydrodynamics, biological communities, marine ecosystem functionality, and air-sea interactions (e.g. Zimmerman and Biggs, 1999; He and Weisberg, 2003; Vukovich, 2007; Molina et al., 2016; Meza-Padilla et al., 2019).

The genesis, evolution, and shedding processes of LCEs have been extensively studied using satellite observations, in situ data (e.g. ocean color satellites, moorings, surface drifters, and pressure inverted echo sounders), numerical simulations, and machine learning techniques (e.g. Vukovich, 1988; Hurlburt and Thompson, 1980; Hamilton, 1992; Hamilton et al., 2002; Lee and Mellor, 2003; DiMarco et al., 2005; Yin and Oey, 2007; Hamilton and Badan, 2009; Chang and Oey, 2012; Le Hénaff et al., 2012; Chang and Oey, 2013a; Xu et al., 2013; Muller-Karger et al., 2015; Liu et al., 2016). In a new study, Zhang et al. (2023) studied the bio-optical properties (chlorophyll-*a* concentration, absorption of particulate and dissolved matters, particulate backscattering, and beam-c attenuation) of an LCE and showed that this eddy has different bio-optical, physical, and chemical properties from the surrounding waters at surface and depth. Several oceanic and atmospheric mechanisms driving LC evolution and LCE shedding were proposed, including variability of the Yucatan Current, instability processes, the momentum balance principle, downstream Florida Strait transport, and topographic influences (Pichevin and Nof, 1997; Hurlburt and Thompson, 1980; Bunge et al., 2002; Oey et al., 2005; Chang and Oey, 2012,

* Corresponding author.
E-mail address: nchaich@ncsu.edu (N. Chaichitehrani).

https://doi.org/10.1016/j.dsr2.2023.105354
Received 20 March 2023; Received in revised form 27 November 2023; Accepted 5 December 2023
Available online 11 December 2023

2013a; Lindo-Atichati et al., 2013; Athié et al., 2020). Oey (2003) and Chang and Oey (2012), for instance, underline the impacts of wind forcing in the GoM and the Caribbean Sea (CS) on the seasonal variability of the LC and LCE shedding process. Furthermore, Chang and Oey (2012, 2013a) reported a biannual increase in LCE shedding in summer and winter. However, significant knowledge gaps exist in understanding the local and remote forcings that contribute to LCE formation and the eddy shedding process. Energetics analysis has been recently proposed as an effective approach to quantitatively describe the energy exchanges between different energy reservoirs (e.g. mean flow and associated eddies) of the LC and other boundary current systems (Oey, 2008; Xu et al., 2013; Elipot and Beal, 2015; Kang and Curchitser, 2015; Brum et al., 2017; Yang and San Liang, 2018; Yan et al., 2019; Zhu et al., 2018; Maslo et al., 2020; Li et al., 2021; Zhang et al., 2022; Huang et al., 2023). An incipient formation and shedding of an eddy occur when energy transfers through barotropic (BT) and baroclinic (BC) instabilities from the main flow to eddies. Alternatively, as energy transfers from the eddies to the main flow, eddies may dissipate (Macdonald et al., 2016). The mechanism of LC ring-shedding was analyzed regarding potential vorticity anomaly and energy transfers by Chérubin et al. (2006) using numerical model results. They confirmed that a mixed barotropic-baroclinic instability is responsible for the LC eddies shedding process (Hurlburt (1985, 1986)), and the BT instability is surface intensified, while the BC instability is intensified in deep layers. Alvera-Azcárate et al. (2009) studied the mesoscale circulation in the Caribbean Sea and the GoM. The barotropic and baroclinic energy conversions were calculated using data from the HYCOM model for the Caribbean Sea. Their results showed that both barotropic and baroclinic energy conversions are positive, transferring energy from the mean flow to the perturbations, and thus allowing the Caribbean eddies to grow.

Donohue et al. (2016) used an array of moored current meters and bottom-mounted pressure inverted echo sounders (PIES) to show that BC instabilities were a significant source of EKE during the formation of three LCEs (Ekman, Franklin, and Hadal) from April 2009 through November 2011 in the Gulf of Mexico. Furthermore, the energetics of the deep GoM was studied in detail by Maslo et al. (2020) using ROMS ocean model outputs. They suggested that eddies are generated by mean circulation in the upper layer, whereas eddies drive mean circulation in the deep layer. They also analyzed that the deep kinetic energy (KE) is maintained by energy transferred from the upper layer to the deep layer by vertical pressure work, by the horizontal pressure work through Yucatan and SoF, and part of this energy is generated through baroclinic instabilities. In addition, in the eastern the Gulf of Mexico, buoyancy conversion has been recognized as the main source of submesoscale kinetic energy in winter (Yang et al., 2021).

Furthermore, Yang et al. (2020) investigated instabilities and multiscale interactions underlying the LC in the GoM using energy budget analysis, and they showed that the canonical energy transfer between the mesoscale eddies and the background flow plays a key role in LCEs shedding. Their energy budget analysis showed that the mesoscale eddy gains energy through barotropic and baroclinic instabilities, which are balanced by horizontal advection, pressure work, and dissipation. Using the global Hybrid Coordinate Ocean Model (HYCOM), Zhang et al. (2022) revealed that BT and BC instabilities of LC and Florida Current system play an important role in the growth and evolution of a frontal eddy ("Tortugas eddy") in the SoF. Moreover, they showed that BC and BT instabilities modulate kinetic and potential energy in this system. Furthermore, the study demonstrated that these instabilities actively modulate the kinetic and potential energy within the system.

Our overarching objective of this study is to understand better EKE and several other key ocean variables and their variations associated with major LCE shedding events identified by long-term drifter observations maintained by Horizon Marine Inc. (Woods Hole Group; https://www.horizonmarine.com/loop-current-eddies). We conducted three specific analyses using long-term ECMWF ERA5 wind data and an ocean reanalysis (ARMOR3D):

1) An energy analysis of the LC system during the shedding of 26 major LCEs ("large" and "huge" eddies as classified by Horizon Marine Inc.) with diameters of 200–400 km (Hamilton et al., 2019) to illuminate the dynamical mechanisms responsible for eddy shedding in the LC system (Section 3.1 and 3.2).
2) An investigation of the variability in Yucatan Channel transport and its correlation with the trade winds in the Caribbean Sea (Section 3.3).
3) Construction of an eddy shedding index (ESI) that links variability among EKE, Yucatan Channel transport, buoyancy frequency, and wind stress for major eddy shedding events (Section 3.4).

2. Data and methods

2.1. Major Gulf of Mexico eddy shedding events

Information about the 26 major LC eddies during 1994–2019 was obtained by combining the historical data compilation by Chang and Oey (2013b) with observations made by Horizon Marine Inc. The primary source of information for EddyWatch is arrays of satellite-tracked drifting buoys. Analysis of drifter tracks for current speed and direction assists in mapping the Loop Current and Loop Current eddies. Drifters in these features provide valuable in situ information on the configuration, orientation of axes, rotation, and current velocities associated with these features. Note that this study focused on separating 26 large and huge LC eddies from the LC, and Table 1 provides information for the separation dates.

2.2. Ocean reanalysis and atmospheric forcing

To analyze internal and external forcing processes affecting the evolution of 26 major LC eddies (huge and large eddies) from 1994 to 2019, we employed ARMOR3D reprocessed monthly simulated salinity, temperature, and geostrophic velocity fields with 1/4° spatial resolution from EU Copernicus Marine Service (Guinehut et al., 2012).

ARMOR3D, a multivariate global ocean state estimate, is constructed by merging mainly Argo-collected vertical temperature and salinity

Table 1
Names, sizes, and shedding dates of 26 major Loop Current eddies (1994–2019) used in the analysis, combined from Chang and Oey (2013b) and Horizon Marine Inc.

Eddy Name	Size	Shedding Date
Yucatan	Large	Sept 1994
Zapp	Large	Mar 1993
Fourchon	Large	Mar 1998
Juggernaut	Huge	Oct 1999
Millennium	Huge	Apr 2001
Pelagic	Huge	Feb 2002
Quick	Huge	Mar 2002
Sargassum	Huge	May 2003
Titanic	Large	Jan 2004
Ulysses	Huge	Sep 2004
Vortex	Huge	Feb 2005
Yankee	Huge	July 2006
Albert	Large	Nov 2007
Brazos	Large	Mar 2008
Cameron	Large	July 2008
Ekman	Huge	July 2009
Franklin	Large	May 2010
Hadal	Huge	Aug 2011
Icarus	Large	Nov 2011
Jumbo	Huge	June 2012
Nautilus	Huge	May 2015
Olympus	Huge	June 2015
Poseidon	Huge	Apr 2016
Quantum	Large	Nov 2017
Revelle	Huge	Apr 2018
Sverdrup	Large	July 2019

profiles with remote sensing observations. The ARMOR3D products are provided by Copernicus Marine Core Service (CMEMS). In addition, along with observations from *in situ* measurements (ships, buoys, and floats) and satellite data, ARMOR3D incorporates more real-time data directly into the analysis, which potentially reduces biases and uncertainties present in conventional numerical models. The ARMOR3D is a data-driven approach that achieves its accuracy by integrating multiple observations and advanced data assimilation techniques. In several studies, the performance of ARMOR3D has been evaluated (Mulet et al., 2012; Barceló-Llull et al., 2018). Mulet et al. (2012) showed that the geostrophic circulation estimated using ARMOR3D has less than 10% errors in the ocean interior. These findings underscore the robustness and reliability of ARMOR3D in capturing the essential dynamics of the ocean. We quality-controlled the utilized products. In addition, sea surface temperature (SST) from ARMOR3D was compared with MODIS-derived SST during eddy shedding events, and relatively a good agreement was observed (not shown here). Since ARMOR3D is not a free-run model, the BT and BC conversions calculated using this dataset must be used with caution (Yang et al., 2020, 2021). While ARMOR3D offers valuable insights, it is essential to consider its limitations. Although the low spatial resolution of ARMOR3D may not capture the LC eddies' details, which may lead to a loss of important features and limit the ability to analyze eddy energetics and eddy energy budgets accurately, since ARMOR3D is a data-driven approach could mitigate these limitations. Monthly data offer a comprehensive overview of oceanic behavior, but it may not capture the full complexity of short-term and rapid energy fluctuations that can significantly impact the dynamics of the system. Monthly data aggregation may smooth out transient events, such as oceanic eddy interactions, which can play a crucial role in energy transfers and conversions. These transient events often operate on shorter timescales than monthly data intervals, potentially leading to an underestimation or misrepresentation of the true magnitude of certain energy transformations.

In addition, the fifth generation of the ECMWF's (European Centre for Medium-Range Weather Forecasts) atmospheric reanalysis global climate dataset (ERA5) hourly wind speed (10 m v and u components) with a horizontal resolution of 0.25° × 0.25° from 1994 to 2019 was obtained from Copernicus Climate Data Store (Mulet et al., 2012; Hersbach et al., 2018; Horányi et al., 2019) for wind stress analysis.

2.3. Zonal wind stress and eddy wind work

Zonal wind stress over the Caribbean Sea and the GoM was computed from 1994 to 2019 to evaluate its possible connection with ocean transport through the Yucatan Channel and with eddy detachments. The zonal and meridional wind stress component (τ_x in Nm^{-2}) for the GoM and the Caribbean Sea was calculated as:

$$\tau_x = \rho C_d U \left(U^2 + V^2\right)^{1/2} \tag{1}$$

$$\tau_y = \rho C_d V \left(U^2 + V^2\right)^{1/2} \tag{2}$$

where ρ is the air density of 1.225 kgm^{-3}, C_d is the empirical drag coefficient of 0.0016 (Petty et al., 2017), and u and v are zonal and meridional wind velocity components at 10 m (from ECMWF ERA5). In addition, the geostrophic eddy wind work (WW; m^3s^{-3}), which explains the energy transfer between wind and ocean, was calculated in the GoM (Renault et al., 2017) as:

$$\mathrm{WW} = \frac{1}{\rho_0}\left(\tau_x^{'} u_g^{'} + \tau_y^{'} v_g^{'}\right) \tag{3}$$

where ρ_0 is the ocean surface density (1027 kg m^{-3}), τ_x and τ_y are the zonal and meridional wind stresses, and u_g and v_g are the zonal and meridional geostrophic currents from ARMOR3D. Note, primes $(\dot{\cdot})$ refer to deviation from the long-term mean (Renault et al., 2017).

2.4. Energy conversion terms

Following Donohue et al. (2016), and to avoid the near-surface subtropical underwater, we performed energetics analysis to quantify mean kinetic energy (MKE), EKE, BT, and BC energy conversion in the LC region (east of 90° W; Fig. 1) at 400 m depth. Based on in situ data, Donohue et al. (2016) showed those clear and strong energy conversions occurred at 400 m depth. As in previous studies (Donohue et al., 2016; Jouanno et al., 2012), these variables were calculated as follows:

$$BT = -\left[u^{'}u^{'}\frac{\partial U_{LP}}{\partial x} + u^{'}v^{'}\left(\frac{\partial U_{LP}}{\partial y} + \frac{\partial V_{LP}}{\partial x}\right) + v^{'}v^{'}\frac{\partial V_{LP}}{\partial y}\right] \tag{4}$$

$$BC = \frac{-g\alpha}{\theta_z} u^{'} T^{'} . \nabla \acute{T} \tag{5}$$

$$EKE = \left(\frac{1}{2}\right)\left(u^{'2} + v^{'2}\right) \tag{6}$$

$$MKE = \left(\frac{1}{2}\right)\left(U_{LP}^2 + V_{LP}^2\right) \tag{7}$$

where u and v are the ARMOR3D x-direction and y-direction velocities, respectively. Following Jouanno et al. (2012), we decomposed current velocity components, where U_{LP} and V_{LP}, representing the mean flow fields, are 120-day low-pass filtered renditions (using a Butterworth filter) of u and v , and $u^{'}$ and $v^{'}$ are the deviation from the mean values that averaged ($u^{'} = u - \overline{u}; v^{'} = v - \overline{v}$) from 1994 to 2009. Since the characteristic periods of LC eddies can vary from a few months to a year, and the lifespans of each 26 LC eddies from genesis, evolution, and dissipation vary widely, the 120-day low-pass filter was applied following Jouanno et al. (2012).

In the BC energy conversion equation (Eq. 4), $T^{'}$ is the temperature anomaly relative to mean water temperature (averaged from 1994 to 2009) at 400 m, $\frac{g\alpha}{\theta_z}$ is estimated as 428 $cm^2s^{-2\circ}C^{-2}$, where g is the acceleration due to gravity, θ_z is the regional background vertical temperature gradient at 400 m depth with a value of 0.023 $^\circ Cm^{-1}$, and α is an effective thermal expansion coefficient ($10^{-4\circ}C^{-1}$; Donohue et al., 2016).

In addition, buoyancy frequency (N^2) was calculated as a measure of water column stratification (e.g. Allahdadi et al., 2017; Koohestani et al., 2021) and BC instabilities in the water column.

$$N^2 = \frac{-g}{\rho_0}\left(\frac{\partial \rho_z}{\partial z}\right) \tag{8}$$

Where water density ρ was calculated using temperature and salinity from ARMOR3D and ρ_0 is the reference seawater density (1025 kgm^3).

We note that positive values of BT (Eq. (3)) indicate a transfer of energy from MKE to EKE (MKE → EKE) through the work of Reynolds stresses against the mean shear. Positive values of BC (Eq. (4)) indicate BC instabilities. Through the mechanism of BC instability, a significant energy transformation occurs within the oceanic system. Mean potential energy (MPE), representing the potential energy associated with large-scale density gradients, undergoes a conversion into eddy potential energy (EPE) through cross-scale energy transfer mechanisms. This transfer contributes to the enhancement of eddy potential energy and reinforces the dynamics of the system. Consequently, buoyancy conversion (EPE → EKE) involves the conversion of potential energy associated with density anomalies and vertical velocity anomalies into eddy kinetic (Zhang et al., 2022; Demyshev et al., 2022; Huang et al., 2023; Demyshev et al., 2022, 2022). The quantification of buoyancy conversion can be derived from observational data, utilizing information about density and vertical velocity anomalies. These processes collectively shape the energy transformations associated with baroclinic instability, contributing to the development and evolution of eddy motions in the

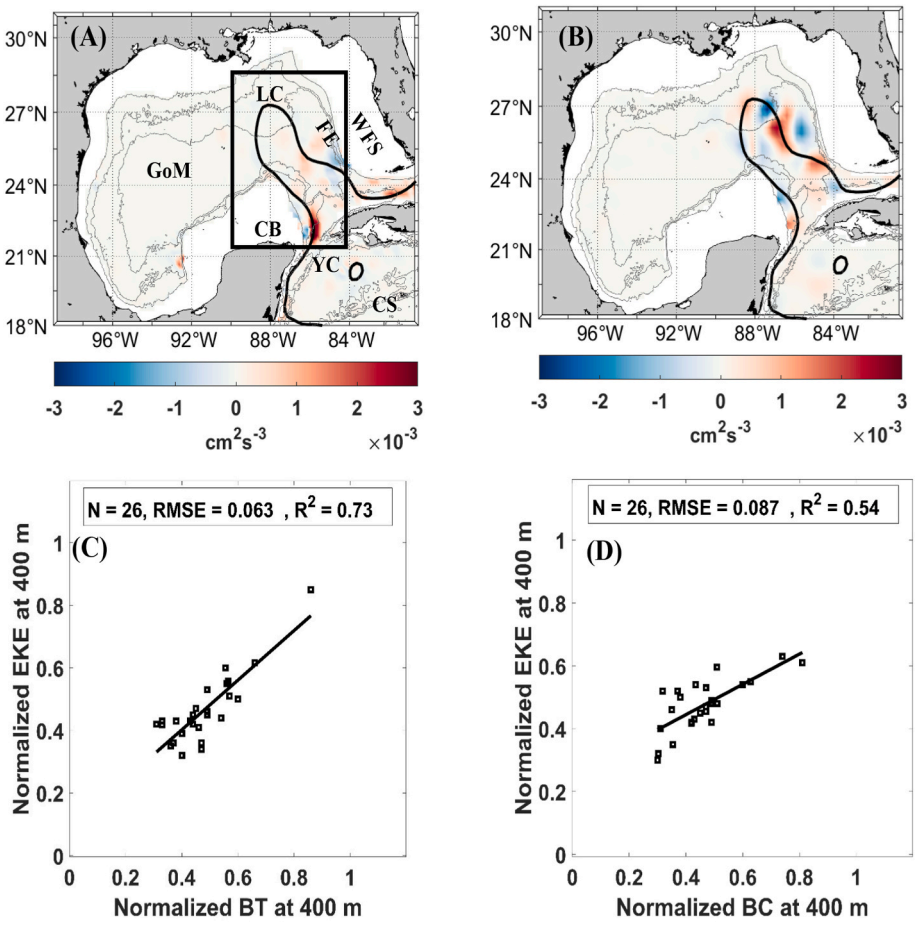

Fig. 1. Three-month average (Apr–Jun 2019) of BT (panel A) and BC (panel B) conversion to EKE of circulation at 400 m before the shedding of eddy Sverdrup (July 2019). The black box in (A) shows the LC active region. The solid black line depicts the mean position of the 17-cm SSH contour, and grey lines indicate the 500, 1500, and 3000 m isobaths. GoM, LC, CB, YC, WFS, CS, and FE stand for the Gulf of Mexico, Loop Current, Campeche Bank, Yucatan Channel, West Florida Shelf, the Caribbean Sea, and Florida Escarpment, respectively. The positive linear correlation between normalized EKE and BT (BC) instability at 400 m is shown in panel C (D) for 26 major LC eddy shedding events.

ocean. Clearly elucidating these energy pathways helps to provide a comprehensive understanding of the dynamics involved in the baroclinic instability phenomenon. Even though BC is related to EPE rather than EKE directly. BC plays a crucial role in the energy conversion process from MPE to EPE, ultimately contributing to EKE generation.

Wang and Pierini (2020) suggested that positive (negative) values of BC tend to increase (decrease) the EKE. Positive values of BC and BT support eddy formation as energy transfers from the mean flow to eddies, whereas negative values indicate energy transfers from eddies to the mean flow as eddies dissipate (e.g. Orlanski and Cox, 1973; Masina et al., 1999; Oey, 2008; Kang and Curchitser, 2015; Wang and Pierini, 2020; Yang et al., 2021).

3. Results

3.1. Barotropic and baroclinic instabilities

The variability of EKE associated with each of the 26 major LC eddies (from 1994 to 2019) was studied with their associated BT and BC instabilities and energy conversion mechanisms. To shed light on the contribution of each mechanism of energy conversion to EKE during the formation and detachment of these major eddies, the EKE was correlated with BT and BC conversion at 400 m (Fig. 1A and B). To do that, BT, BC, and EKE were calculated, normalized, and averaged over the LC active region, which is east of 90 °*W* (denoted by the black box in Fig. 1C), where LC and LCEs are most commonly located (e.g. Garcia-Jove et al., 2016). The normalization was performed by deducting the minimum value of the variable from the variable to be normalized, and the result was divided by the range of the variable. This normalization procedure was important as it allows different ocean environmental variables to have the same scale and be comparable.

BT and BC have drastically different spatial characteristics in the study period. For instance, the 400 m BC and BT before the shedding of Eddy Sverdrup (July 2019, Fig. 1A and B) reveal that high loading of BT is distributed in the southwestern part of the LC active area, with peak values centered at the Yucatan Strait and the shelf break of the Campeche Bank. In contrast, high-loading BC instabilities are located near the Florida Escarpment and in the central portion of the LC active area, having localized, alternating eddy features. The observed spatial variabilities of BT and BC instabilities are consistent with Yang et al. (2020). Energy transfers to the LC eddies are thus through both BT and BC pathways. Taking all 26 major eddy shedding events into consideration, we found a positive linear correlation between EKE, BC, and BT (Fig. 1C and D), indicating that both BT and BC instabilities contribute to the increase in EKE during major eddy shedding events. EKE is correlated more with BT.

($R^2 = 0.73, p - value = 0.0093$) than with BC ($R^2 = 0.54, p - value = 0.042$), suggesting that BT is a more efficient pathway than BC in EKE generation. The Mann–Kendall test (Mann, 1945; Kendall, 1975; Androulidakis and Krestenitis, 2022; Brkić, 2023) was employed to calculate the p values. In this test, a p value of less than 0.05 was considered statistically significant (Androulidakis and Krestenitis,

2022). Thus, we can confidently conclude that the correlations observed in this study are statistically significant according to the Mann–Kendall test.

3.2. Co-variability of EKE, BT, BC, and MKE

The co-variabilities of normalized EKE, MKE, BT, and BC of the low-pass filtered current at 400 m depth in 1994–2019 are depicted in Fig. 2. As expected, an increase in EKE was observed during each eddy shedding event (Fig. 2A). Timeseries of BT and BC (Fig. 2B and C) allow us to investigate the energy exchanges between each reservoir. The time series of BT and BC (Fig. 2B and C) elucidates that instability in BT and BC triggered the eddy shedding processes. The time series of BT at 400 m depth explains the exchange of energy with the kinetic energy of currents during our analysis period, and eddy shedding events (Fig. 2B, dashed red lines), and elevated values of BT describe the conversion of energy through BT instabilities. BC instabilities were strengthened during some eddy shedding events (Fig. 2C; dashed red lines). EKE was strengthened during eddy shedding events as the mean flow became more barotropically or baroclinically unstable. Our results reveal that BT instability led to EKE growth, and BC led to the growth of EPE directly and influenced EKE growth indirectly during the generation and separation of LC eddies. The observed mixed instability in our analysis agrees with previous studies (Hurlburt, 1985, 1986). The increased energy flux from MKE to EKE, as seen in the time series of MKE at 400 m depth (Fig. 2D), led to elevated EKE in the month proceeding or during eddy shedding events. The observed peaks in EKE, BT, and BC, which have not been marked in Fig. 2, could be due to eddies' detachment-reattachment events that may occur multiple times (Hamilton et al., 2019; Nickerson et al., 2022). Note, the investigation of the LC eddies' detachment-reattachment events was beyond the scope of this study.

3.3. YC transport, wind stress, and N2

Our analysis advances the idea that YC transport variations enhance BT instability (Fig. 3A), efficiently releasing energy from MKE to EKE through the BT energy pathway, ultimately leading to eddy shedding. In addition, the relationships between normalized YC transport and normalized τ_x along with the normalized BC and normalized N^2_{max} have been investigated (Fig. 3B–D). Yang et al. (2017) showed that the Kuroshio extension's strong meanderings prompt BT transfers from MKE to EKE, resulting in increased eddy activity. Nearly the same pattern was observed in the GoM, as YC transport triggers BT instabilities and energetic conversion. The normalized YC transport exhibits a positive correlation

($R^2 = 0.60, p - value = 0.023$) with normalized BT (Fig. 3A). In addition, the positive correlation ($R^2 = 0.69, p - value = 0.039$) between easterly wind over the Caribbean Sea and YC transport during major eddy shedding events (Fig. 3B) supports findings of earlier studies (e.g. Chang and Oey, 2012, 2013a, b) that the easterly wind over the Caribbean Sea modulates YC transport. The monthly time series of normalized τ_x over the Caribbean Sea and normalized YC transport for 1994–2019 clearly suggests that wind forcing over the Caribbean Sea (leading by one month) controls YC transport (Fig. 3D). To investigate what modulates BC instability in the eastern Gulf of Mexico, buoyancy frequency (N^2) was used to investigate BC instabilities in buoyancy-driven flow (Hetland, 2017). The normalized BC transport exhibits a negative correlation ($R^2 = -0.52, p - value = 0.0014$) with normalized N^2_{max}. N^2 is used as a measure of stratification. An increase (decrease) in N^2 indicates the water column is more (less) stratified. Vallis (2017) showed that baroclinic instability prevails when vertical stratification weakens. Ayouche et al. (2021) showed that the stratification decreases after a wind event in the North-East Atlantic Ocean, and baroclinic instabilities increase. The negative linear correlation between LC region-averaged and 3-month averaged (prior to eddy shedding events) BC and N^2_{max} shows that as N^2_{max} decreases, the water column becomes baroclinically unstable right before eddy shedding (Fig. 3C).

The relationship between MKE, which leads by one month, and EKE during eddy shedding events ($R^2 = 0.60, p - value = 0.0044$) is presented in Fig. 4A. Since the YC transport variations effectively induce BT instability and energy transfer from MKE to EKE, the connection between the YC transport and MKE is expected. The positive relationship between the YC transport and MKE for a month before eddy shedding events

($R^2 = 0.56, p - value = 0.011$), as shown in Fig. 4B. Our results are consistent with previous studies, showing the positive relationships between lead-lag MKE and EKE, and MKE with the mean flow (Jouanno et al., 2009, 2012; Hao et al., 2022). Hence, we can assert that the correlations observed in this study exhibit statistical significance, as indicated by the Mann–Kendall test with a p-value of less than 0.05.

3.4. Wind stress and wind stress work

We investigated and quantified the work done by wind stress (Eq. (2)) over the GoM on LC eddies. Xu et al. (2016) quantified wind stress and its negative work done on the development of oceanic mesoscale eddies in most oceanic regions using satellite observations. They also

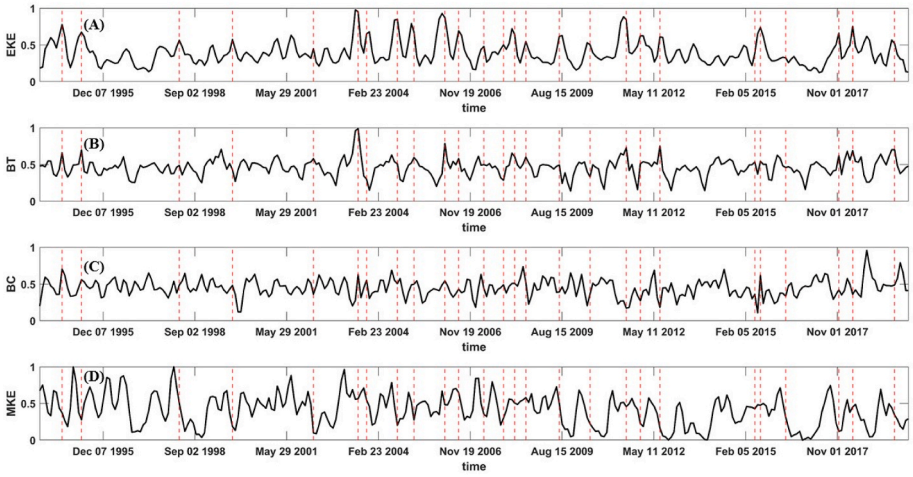

Fig. 2. Time series of low-pass filtered LC region-mean normalized (A) EKE, (B) BT, (C) BC, and (D) MKE at 400 m. Red dashed lines indicate 26 major eddy shedding events.

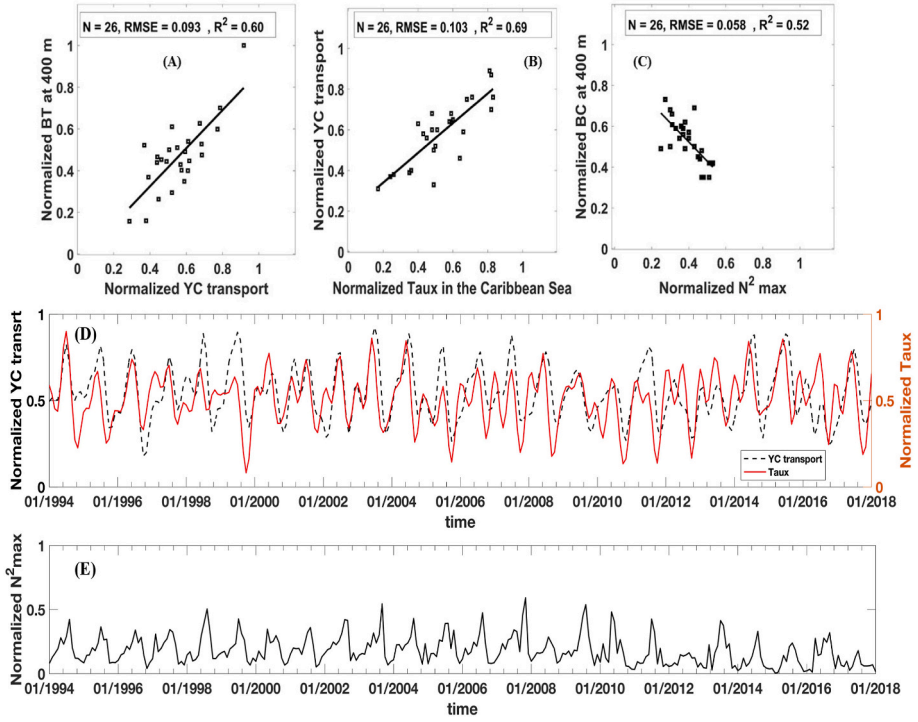

Fig. 3. (A) The positive linear correlation between spatially averaged (over the LC region), temporally averaged (for three months), normalized BT at 400 m and normalized YC transport. (B) The correlation between normalized YC transport and normalized zonal wind stress (τ_x) in the Caribbean Sea for 26 major LC eddy shedding events. (C) The negative linear correlation between normalized BC at 400 m and N^2_{max}. (D) Time series of the normalized YC transport (dashed black line) and normalized τ_x in the Caribbean Sea (solid red line) from Jan. 1994–Dec. 2019 (E) Time series of the normalized N^2_{max} from Jan. 1994–Dec. 2019.

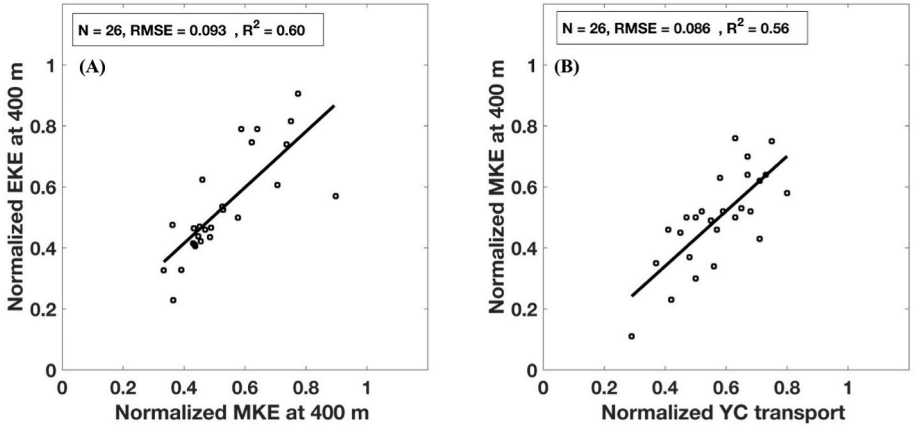

Fig. 4. The positive linear correlation between (A) normalized MKE (leads by a month) and normalized EKE at 400 m during 26 major LC eddy shedding events and (B) normalized YC transport and MKE at 400, for a month before eddy shedding events.

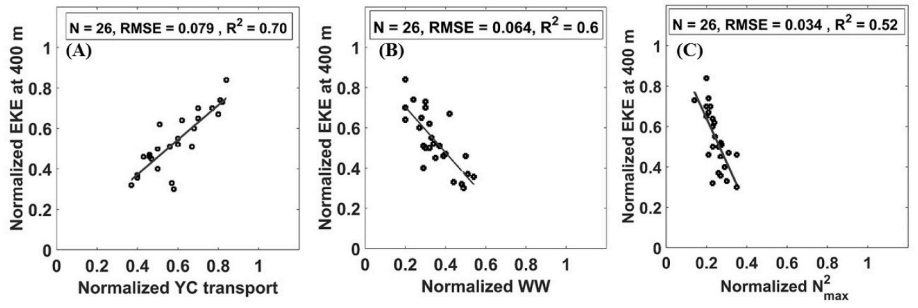

Fig. 5. The correlations between normalized EKE and (A) normalized YC transport, (B) normalized *WW*, and (C) normalized N^2_{max} for 26 major LC eddy shedding events.

showed the linear relationship between wind stress curl and wind stress work (WW). Our findings (Fig. 5B) indicate that the wind stress work over the GoM is negative during the eddy shedding events. The inverse relationship between WW and EKE.

($R^2 = -0.6, p - value = 0.003$) suggests that the wind stress over the GoM inhibits the development of eddies. In other words, as wind stress increases, the work done by wind has negative, systematic, and direct impact on eddy energetics, which leads to removing eddy energy and a decrease in EKE over the LC region. Our result is consistent with previous numerical modeling studies, which suggested that EKE decreases when the eddy damping by the relative wind stress work was included (Eden and Dietze, 2009; Munday and Zhai, 2015). In addition, we can confidently affirm that the correlations observed in this study demonstrate statistical significance, as evidenced by the Mann–Kendall test (p-value <0.05).

3.5. Predictability of EKE: Eddy shedding index

One of the goals of this work was to develop an index that could be used to estimate EKE in the GoM during major eddy shedding events. As mentioned in sections 3.1 and 3.2, energy from the LC transfers to eddies through BT and BC energy pathways, resulting in an increase in EKE and EPE during eddy shedding events (Fig. 1). We also discussed the YC transport variables and N^2_{max} indirectly impact eddy energetics (here, EKE) by modulating BT and BC instabilities, respectively. In addition, the direct negative effects of WW on EKE were shown (Fig. 5B), which explains the negative work done by wind stress on eddies resulting in decreasing EKE. Here, we used these three variables that directly (WW) and indirectly (YC transport and N^2_{max}) modulate EKE to estimate EKE during major eddy shedding events in the GoM. The index would then facilitate the prediction of eddy shedding. We simply formulated an Eddy Shedding Index (ESI) using EKE, *WW* over the eastern GoM (the LC region), YC transport, and N^2_{max} over the eastern GoM (the LC region) using the Statistics Toolbox in MATLAB:

$$ESI = 0.7947 - 1.0784 \times N^2_{max} - 0.5954 \times WW + 0.3657 \times YCtransport \quad (9)$$

The three coefficients of the variables and the constant value were determined simply by using linear regression.

Our results showed that EKE at 400 m is positively correlated with 1-month shifted YC transport ($R^2 = 0.70, p - value = 0.006$) (Fig. 5A) and negatively correlated with *WW* and N^2 *max* in the GoM Fig. 5B and C). By calculating the ESI when each of the 26 historical major eddies separated from the LC, the threshold value for eddy separation was found to be 0.46 (Fig. 6).

4. Discussion and conclusions

Our analysis focused on 26 major LC eddies energy exchanges associated with BT and BC instabilities in the LC region of the GoM using ARMOR3D. Results show that EKE grows through BT and BC instabilities. EKE measures the intensity of mesoscale eddy activity. Furthermore, our analysis indicates that BC and BT energy transfer processes are important in generating LC eddies.

The conversion of MKE to EKE becomes evident in the LC region during major eddy shedding events. Our results support that MKE is higher prior to or during shedding, and as MKE is converted to EKE during shedding, MKE subsequently decreases. Furthermore, analysis of the time series of EKE confirms that EKE increases during eddy shedding events through either the baroclinic BC pathway, the BT pathway, or a combination of both. Moreover, our analysis demonstrates that BC and BT instabilities exhibit different patterns of increase within various regions of the LC. Notably, along the southern edge of the LC, adjacent to the Campeche Bank, high BT instabilities are prominently observed ($>3 \times 10^{-3} cm^2 s^{-3}$).

BT instabilities are enhanced by extracting kinetic energy from the horizontally sheared YC transport, which feeds the LC. The positive linear correlation observed between BT instabilities and YC transport, as well as between EKE and YC transport, provide further evidence that the intensified YC transport enhances BT instabilities and contributes to EKE within the LC system. In addition, YC transport could modulate EKE fluctuations primarily through its direct impact on BT. For future studies, we recommend investigating the influence of YC transport on BT and EKE fluctuations using higher spatial (<10 km) and temporal resolution. In addition, we recommend employing ocean model data (e.g. HYCOM) data to assess their efficacy in conducting energy budget analyses during eddy shedding events for a wide range of eddy sizes. Additionally, it is worth considering the integration of artificial intelligence (AI) techniques that incorporate ocean model data and observations for calculating ESI.

The relationship between easterly wind stress over the Caribbean Sea and YC transport has been demonstrated multiple times (Oey and Lee, 2002; Ezer et al., 2003; Chang and Oey, 2012; Athié et al., 2020). Furthermore, Chang and Oey (2012, 2013a, b) showed that easterly wind over the Caribbean Sea modulates YC transport, LC intrusion into the GoM, and ultimately LC eddy shedding. Considering the complex dynamics of easterly wind in the Caribbean Sea and YC transport, it is imperative to investigate whether the present analyses support the deterministic relationship between easterly wind stress over the Caribbean Sea and YC transport. The YC transport exhibits a strong positive correlation ($R^2 = 0.69$) with easterly zonal wind stress in the Caribbean Sea during eddy shedding. The increase in YC transport promotes deeper penetration of the LC into the GoM. Our results showed that there was an increase in YC transport a month prior to the release of eddies. Hence, the energy source for eddy formation through BT conversion could come from external forcing that originated in the Caribbean Sea.

Our results confirmed that BC instabilities associated with vertical shear of the mean flow are prominent in the northern and eastern parts of the LC. The inverse relationship between BC instabilities and N^2_{max} supports the idea that buoyancy inputs force BC instabilities. A decrease in N^2 indicates that stratification weakens and would be more favorable for BC instabilities, which leads to eddy activity. In addition, BC instabilities can be viewed as vertical shear instability, through which potential energy converts to EKE. LCEs may detach and reattach to the LC multiple times. This may amplify BC instabilities and promote multiple eddy detachments.

We developed an Eddy Shedding Index (ESI) to predict eddy shedding in the LC region. YC transport, *WW*, and N^2_{max}, which control BT and BC instabilities, were used to construct the index. *WW* and N^2_{max} were computed over the LC region. The positive correlation between EKE and YC transport reveals that the intrusion of YC transport into the GoM

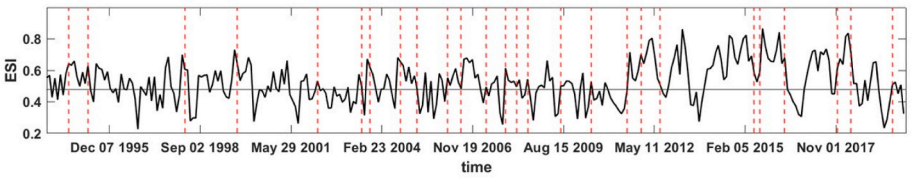

Fig. 6. Time series of the Eddy Shedding Index (ESI, solid black line). The red dashed vertical lines indicate major eddy shedding events, and the horizontal grey line indicates the threshold value (0.46).

plays a key role in energy conversion. Moreover, the inverse linear relationship between EKE and *WW* underlines that eddy activities are significantly dampened by strong wind and current feedback (Renault et al., 2017). Our newly developed ESI can predict future major LCE shedding when ESI exceeds the threshold value (0.46).

CRediT authorship contribution statement

Nazanin Chaichitehrani: Data curation, Formal analysis, Investigation, Methodology, Validation, Visualization, Writing – original draft, Writing – review & editing. **Ruoying He:** Conceptualization, Funding acquisition, Supervision.

Declaration of competing interest

I have read and understood the Deep Sea Research Journal policy on the declaration of interests. I hereby declare that we have no pecuniary or other personal interest, direct or direct, in any matter that raises or may raise a conflict.

Data availability

Data will be made available on request.

Acknowledgments

This study was supported by the Gulf Research Program of the National Academies of Sciences, Engineering, and Medicine under award number 2000009966. We thank Horizon Marine Inc for providing historical Loop Current Eddy information online at https://www.horizonmarine.com/loop-current-eddies. We thank Jennifer Warrillow for editing this paper.

References

Allahdadi, M.N., Li, C., 2017. Numerical experiment of stratification induced by diurnal solar heating over the Louisiana Shelf. In: Justic, D., Rose, K.A., Hetland, R.D., Fennel, K. (Eds.), Modeling Coastal Hypoxia. Springer, Cham, pp. 1–22. https://doi.org/10.1007/978-3-319-54571-4_1.

Alvera-Azcárate, A., Barth, A., Weisberg, R.H., 2009. The surface circulation of the Caribbean Sea and the Gulf of Mexico as inferred from satellite altimetry. J. Phys. Oceanogr. 39, 640–657. https://doi.org/10.1175/2008JPO3765.1.

Androulidakis, Y.S., Krestenitis, Y.N., 2022. Sea surface temperature variability and marine heat waves over the Aegean, Ionian, and Cretan Seas from 2008–2021. J. Mar. Sci. Eng. 10, 42. https://doi.org/10.3390/jmse10010042.

Athié, G., Sheinbaum, J., Candela, J., Ochoa, J., Pérez-Brunius, P., Romero-Arteaga, A., 2020. Seasonal variability of the transport through the Yucatan Channel from observations. J. Phys. Oceanogr. 50 (2), 343–360. https://doi.org/10.1175/JPO-D-18-0269.1.

Ayouche, A., Charria, G., Carton, X., Ayoub, N., Theetten, S., 2021. Non-linear processes in the Gironde River plume (north-east Atlantic): instabilities and mixing. Front. Mar. Sci. 8 https://doi.org/10.3389/fmars.2021.701773.

Barceló-Llull, B., Pascual, A., Mason, E., Mulet, S., 2018. Comparing a multivariate global ocean state estimate with high-resolution in situ data: an anticyclonic intrathermocline eddy near the Canary Islands. Front. Mar. Sci. 5 https://doi.org/10.3389/fmars.2018.00066.

Brkić, Ž., 2023. Increasing water temperature of the largest freshwater lake on the Mediterranean islands as an indicator of global warming. Heliyon 9, e19248. https://doi.org/10.1016/j.heliyon.2023.e19248.

Brum, A.L., de, Azevedo, J.L.L., de, Oliveira, L.R., Calil, P.H.R., 2017. Energetics of the Brazil current in the Rio Grande Cone region. Deep Sea Res. Part II. Oceanogr. 128, 67–81. https://doi.org/10.1016/j.dsr.2017.08.014.

Bunge, L., Ochoa, J., Badan, A., Candela, J., Sheinbaum, J., 2002. Deep flows in the Yucatan Channel and their relation to changes in the Loop Current extension. J. Geophys. Res. Oceans 107. https://doi.org/10.1029/2001JC001256, 26-1-26–7.

Chang, Y.-L., Oey, L.-Y., 2011. Loop Current cycle: coupled response of the Loop Current with deep flows. J. Phys. Oceanogr. 41 (3), 458–471. https://doi.org/10.1175/2010JPO4479.1.

Chang, Y.-L., Oey, L.-Y., 2012. Why does the Loop Current tend to shed more eddies in summer and winter?: seasonal Loop Current shedding. Geophys. Res. Lett. 39 (5) https://doi.org/10.1029/2011GL050773.

Chang, Y.-L., Oey, L.-Y., 2013a. Loop Current growth and eddy shedding using models and observations: numerical process experiments and satellite altimetry data. J. Phys. Oceanogr. 43 (3), 669–689. https://doi.org/10.1175/JPO-D-12-0139.1.

Chang, Y.-L., Oey, L.-Y., 2013b. Coupled response of the trade wind, sst gradient, and sst in the Caribbean Sea, and the potential impact on Loop Current's interannual variability. J. Phys. Oceanogr. 43 (7), 1325–1344. https://doi.org/10.1175/JPO-D-12-0183.1.

Chérubin, L.M., Morel, Y., Chassignet, E.P., 2006. Loop Current ring shedding: the formation of cyclones and the effect of topography. J. Phys. Oceanogr. 36, 569–591. https://doi.org/10.1175/JPO2871.1.

Demyshev, S., Dymova, O., Miklashevskaya, N., 2022. Seasonal variability of the dynamics and energy transport in the Black Sea by simulation data. Water 14, 338. https://doi.org/10.3390/w14030338.

DiMarco, S.F., Nowlin Jr., W.D., Reid, R.O., 2005. A statistical description of the velocity fields from upper ocean drifters in the Gulf of Mexico. In: Sturges, W., Lugo Fernandez, A. (Eds.), Geophys. Monogr. Ser., vol. 161. AGU, Washington, D. C, pp. 101–110. https://doi.org/10.1029/161GM08.

Donohue, K.A., Watts, D.R., Hamilton, P., Leben, R., Kennelly, M., 2016. Loop Current Eddy formation and baroclinic instability. Dynam. Atmos. Oceans 76, 195–216. https://doi.org/10.1016/j.dynatmoce.2016.01.004.

Eden, C., Dietze, H., 2009. Effects of mesoscale eddy/wind interactions on biological new production and eddy kinetic energy. J. Geophys. Res. Oceans 114, C05023. https://doi.org/10.1029/2008JC005129.

Elipot, S., Beal, L.M., 2015. Characteristics, energetics, and origins of Agulhas Current Meanders and their limited influence on ring shedding. J. Phys. Oceanogr. 45 (9), 2294–2314. https://doi.org/10.1175/JPO-D-14-0254.1.

Ezer, T., Oey, L.-Y., Lee, H.-C., Sturges, W., 2003. The Variability of currents in the Yucatan Channel: analysis of results from a numerical ocean model. J. Geophys. Res. Oceans 108. https://doi.org/10.1029/2002JC001509.

Fratantoni, P.S., Lee, T.N., Podesta, G.P., Muller-Karger, F., 1998. The influence of Loop Current perturbations on the formation and evolution of Tortugas eddies in the southern Straits of Florida. J. Geophys. Res. Oceans 103, 24759–24779. https://doi.org/10.1029/98JC02147.

Garcia-Jove, M., Sheinbaum, J., Jouanno, J., Garcia-Jove, M., Sheinbaum, J., Jouanno, J., 2016. Sensitivity of Loop Current metrics and eddy detachments to different model configurations: the impact of topography and Caribbean perturbations. Atmósfera 29 (3), 235–265. https://doi.org/10.20937/ATM.2016.29.03.05.

Guinehut, S., Dhomps, A.-L., Larnicol, G., Le Traon, P.-Y., 2012. High resolution 3-D temperature and salinity fields derived from in situ and satellite observations. Ocean Sci. 8 (5), 845–857. https://doi.org/10.5194/os-8-845-2012.

Hamilton, P., 1990. Deep currents in the Gulf of Mexico. J. Phys. Oceanogr. 20, 1087–1104. https://doi.org/10.1175/1520-0485(1990)020<1087:DCITGO>2.0.CO;2.

Hamilton, P., 1992. Lower continental slope cyclonic eddies in the central Gulf of Mexico. J. Geophys. Res. Oceans 97, 2185–2200. https://doi.org/10.1029/91JC01496.

Hamilton, P., Badan, A., 2009. Subsurface jets in the northwestern Gulf of Mexico. J. Phys. Oceanogr. 39, 2875–2891. https://doi.org/10.1175/2009JPO4158.1.

Hamilton, P., Berger, T.J., Johnson, W., 2002. On the structure and motions of cyclones in the northern Gulf of Mexico. J. Geophys. Res. Oceans 107. https://doi.org/10.1029/1999JC000270, 1-1-1–18.

Hamilton, P., Bower, A., Furey, H., Leben, R., Pérez-Brunius, P., 2019. The Loop Current: observations of deep eddies and topographic waves. J. Phys. Oceanogr. 49, 1463–1483. https://doi.org/10.1175/JPO-D-18-0213.1.

Hao, Z., Xu, Z., Feng, M., Zhang, P., Yin, B., 2022. Dynamics of interannual eddy kinetic energy variability in the Sulawesi Sea revealed by OFAM3. J. Geophys. Res. Oceans 127, e2022JC018815. https://doi.org/10.1029/2022JC018815.

He, R., Weisberg, R.H., 2003. West Florida shelf circulation and temperature budget for the 1998 fall transition. Continent. Shelf Res. 23 (8), 777–800. https://doi.org/10.1016/S0278-4343(03)00028-1.

Hersbach, H., de Rosnay, P., Bell, B., Schepers, D., Simmons, A., Soci, C., et al., 2018. Operational Global Reanalysis: Progress, Future Directions and Synergies with NWP. ECMWF. https://doi.org/10.21957/tkic6g3wm.

Hetland, R.D., 2017. Suppression of baroclinic instabilities in buoyancy-driven flow over sloping bathymetry. J. Phys. Oceanogr. 47, 49–68. https://doi.org/10.1175/JPO-D-15-0240.1.

Hirschi, J.J.-M., Frajka-Williams, E., Blaker, A.T., Sinha, B., Coward, A., Hyder, P., et al., 2019. Loop Current variability as trigger of coherent Gulf Stream transport anomalies. J. Phys. Oceanogr. 49 (8), 2115–2132. https://doi.org/10.1175/JPO-D-18-0236.1.

Horányi, A., Muñoz Sabater, J., Nicolas, J., Peubey, C., Radu, R., Rozum, I., Schepers, D., Simmons, A., Soci, C., Dee, D., Thépaut, J.-N., 2019. ERA5 Monthly Averaged Data on Single Levels from 1979 to Present. https://cds.climate.copernicus.eu/cdsapp#!/dataset/reanalysis-era5-single-levels-monthly-means?tab=form/. (Accessed 19 October 2021).

Huang, M., Yang, Y., Liang, X., 2023. Seasonal eddy variability in the northwestern tropical Atlantic Ocean. J. Phys. Oceanogr. 53, 1069–1085. https://doi.org/10.1175/JPO-D-22-0200.1.

Hurlburt, H.E., 1985. Cyclonic eddy generation in the Gulf of Mexico. Proc. Sixth annual Gulf of Mexico information transfer meeting, Gulf of Mexico OCS regional office, minerals management Service. U.S. Dept. of the Interior 272– 273, 283.

Hurlburt, H.E., 1986. Dynamic transfer of simulated altimeter data into subsurface information by a numerical ocean model. J. Geophys. Res. Oceans 91, 2372–2400. https://doi.org/10.1029/JC091iC02p02372.

Hurlburt, H.E., Thompson, J.D., 1980. A Numerical study of Loop Current intrusions and eddy shedding. J. Geophys. Res. Oceans 10 (10), 1611–1651. https://doi.org/10.1175/1520-0485(1980)010<1611:ANSOLC>2.0.CO;2.

Jouanno, J., Sheinbaum, J., Barnier, B., Molines, J.-M., 2009. The mesoscale variability in the Caribbean Sea. Part II: energy sources. Ocean Model. 26 (3), 226–239. https://doi.org/10.1016/j.ocemod.2008.10.006.

Jouanno, J., Sheinbaum, J., Barnier, B., Molines, J.M., Candela, J., 2012. Seasonal and interannual modulation of the eddy kinetic energy in the Caribbean Sea. J. Phys. Oceanogr. 42, 2041–2055. https://doi.org/10.1175/JPO-D-12-048.1.

Kang, D., Curchitser, E.N., 2015. Energetics of eddy–mean flow interactions in the Gulf Stream region. J. Phys. Oceanogr. 45 (4), 1103–1120. https://doi.org/10.1175/JPO-D-14-0200.1.

Kendall, M., 1975. Rank Correlation Measures. Charles Griffin, London, UK.

Koohestani, K., Allahdadi, M.N., Chaichitehrani, N., 2021. Oceanic response to Tropical Cyclone Gonu (2007) in the Gulf of Oman and the Northern Arabian Sea: estimating depth of the mixed layer using satellite sst and climatological data. J. Mar. Sci. Eng. 9 (11), 1244. https://doi.org/10.3390/jmse9111244.

Le Hénaff, M., Kourafalou, V.H., Morel, Y., Srinivasan, A., 2012. Simulating the dynamics and intensification of cyclonic Loop current frontal eddies in the Gulf of Mexico. J. Geophys. Res. Oceans 117. https://doi.org/10.1029/2011JC007279.

Leben, R.R., 2005. Altimeter-derived Loop current metrics. In: Sturges, W., Lugo Fernandez, A. (Eds.), Circulation in the Gulf of Mexico: Observations and Models, Geophys. Monogr. Ser., vol. 161. AGU, Washington, D. C, pp. 181–201. https://doi.org/10.1029/161GM15.

Lee, H.-C., Mellor, G.L., 2003. Numerical simulation of the Gulf Stream system: the Loop current and the deep circulation. J. Geophys. Res. Oceans 108. https://doi.org/10.1029/2001JC001074.

Li, J., Roughan, M., Kerry, C., 2021. Dynamics of interannual eddy kinetic energy modulations in a Western Boundary Current. Geophys. Res. Lett. 48, e2021GL094115 https://doi.org/10.1029/2021GL094115.

Lindo-Atichati, D., Bringas, F., Goni, G., 2013. Loop Current excursions and ring detachments during 1993–2009. Int. J. Rem. Sens. 34 (14), 5042–5053. https://doi.org/10.1080/01431161.2013.787504.

Liu, Y., Weisberg, R.H., Vignudelli, S., Mitchum, G.T., 2016. Patterns of the Loop Current system and regions of sea surface height variability in the eastern Gulf of Mexico revealed by the self-organizing maps. J. Geophys. Res. Oceans 121, 2347–2366. https://doi.org/10.1002/2015JC011493.

Macdonald, H., Roughan, M., Baird, M., Wilkin, J., 2016. The formation of a cold-core eddy in the East Australian Current. Continent. Shelf Res. 114, 72–84. https://doi.org/10.1016/j.csr.2016.01.002.

Mann, H.B., 1945. Nonparametric tests against trend. J. Econom. Soc. 13, 245–259.

Masina, S., Philander, S.G.H., Bush, A.B.G., 1999. An analysis of tropical instability waves in a numerical model of the Pacific Ocean: 2. Generation and energetics of the waves. J. Geophys. Res. Oceans 104 (29). https://doi.org/10.1029/1999JC900226, 637-29, 661.

Maslo, A., Souza, J.M.A.C. de, Pardo, J.S., 2020. Energetics of the deep Gulf of Mexico. J. Phys. Oceanogr. 50, 1655–1675. https://doi.org/10.1175/JPO-D-19-0308.1.

Meza-Padilla, R., Enriquez, C., Liu, Y., Appendini, C.M., 2019. Ocean circulation in the western Gulf of Mexico using self-organizing maps. J. Geophys. Res. Oceans 124 (6), 4152–4167. https://doi.org/10.1029/2018JC014377.

Molina, M.J., Timmer, R.P., Allen, J.T., 2016. Importance of the Gulf of Mexico as a climate driver for U.S. severe thunderstorm activity. Geophys. Res. Lett. 43 (23) https://doi.org/10.1002/2016GL071603.

Mulet, S., Rio, M.-H., Mignot, A., Guinehut, S., Morrow, R., 2012. A new estimate of the global 3D geostrophic ocean circulation based on satellite data and in-situ measurements. Deep-Sea Res. II: Top. Stud. Oceanogr. 77–80, 70–78. https://doi.org/10.1016/j.dsr2.2012.04.012.

Muller-Karger, F.E., Smith, J.P., Werner, S., Chen, R., Roffer, M., Liu, Y., Muhling, B., Lindo-Atichati, D., Lamkin, J., Cerdeira-Estrada, S., Enfield, D.B., 2015. Natural variability of surface oceanographic conditions in the offshore Gulf of Mexico. Prog. Oceanogr. 134, 54–76. https://doi.org/10.1016/j.pocean.2014.12.007.

Munday, D.R., Zhai, X., 2015. Sensitivity of Southern Ocean circulation to wind stress changes: role of relative wind stress. Ocean Model. 95, 15–24. https://doi.org/10.1016/j.ocemod.2015.08.004.

Nickerson, A.K., Weisberg, R.H., Liu, Y., 2022. On the evolution of the Gulf of Mexico Loop Current through its penetrative, ring shedding and retracted states. Adv. Space Res. 69, 4058–4077. https://doi.org/10.1016/j.asr.2022.03.039.

Oey, L.-Y., 2003. Effects of winds and Caribbean eddies on the frequency of Loop Current eddy shedding: a numerical model study. J. Geophys. Res. Oceans 108 (C10), 3324. https://doi.org/10.1029/2002JC001698.

Oey, L.-Y., 2008. Loop Current and deep eddies. J. Phys. Oceanogr. 38 (7), 1426–1449. https://doi.org/10.1175/2007JPO3818.1.

Oey, L.-Y., Lee, H.-C., 2002. Deep eddy energy and topographic Rossby waves in the Gulf of Mexico. J. Phys. Oceanogr. 32, 3499–3527. https://doi.org/10.1175/1520-0485(2002)032<3499:DEEATR>2.0.CO;2.

Oey Jr., L.-Y., Ezer, T., Lee, H.-C., 2005. Loop Current, rings and related circulation in the Gulf of Mexico: a review of numerical models and future challenges. In: Sturges, W., Lugo Fernandez, A. (Eds.), Circulation in the Gulf of Mexico: Observations and Models, Geophys. Monogr. Ser., vol. 161. AGU, Washington, D. C, pp. 31–56. https://doi.org/10.1029/161GM04.

Orlanski, I., Cox, M.D., 1973. Baroclinic instability in ocean currents. Geophys. Fluid Dynam. 4 (4), 297–332. https://doi.org/10.1080/03091927208236102.

Petty, A.A., Tsamados, M.C., Kurtz, N.T., 2017. Atmospheric form drag coefficients over Arctic sea ice using remotely sensed ice topography data, spring 2009–2015. J. Geophys. Res. Earth Surf. 122 (8), 1472–1490. https://doi.org/10.1002/2017JF004209.

Pichevin, T., Nof, D., 1997. The momentum imbalance paradox. Tellus 49 (2), 298–319. https://doi.org/10.1034/j.1600-0870.1997.t01-1-00009.x.

Reid, R.O., 1972. A simple dynamic model of the Loop Current. In: Capurro, L.R.A., Reid, J.L. (Eds.), Contributions to the Physical Oceanography of the Gulf of Mexico, vol. 2. Texas A & M University Oceanography Studies, College Station, TX, pp. 3–64.

Renault, L., McWilliams, J.C., Masson, S., 2017. Satellite observations of imprint of oceanic current on wind stress by air-sea coupling. Sci. Rep. 7 (1), 17747 https://doi.org/10.1038/s41598-017-17939-1.

Sturges, W., Leben, R., 2000. Frequency of ring separations from the Loop Current in the Gulf of Mexico: a revised estimate. J. Phys. Oceanogr. 30 (7), 1814–1819. https://doi.org/10.1175/1520-0485(2000)030<1814:FORSFT>2.0.CO;2.

Vallis, G.K., 2017. Atmospheric and Oceanic Fluid Dynamics, second ed. Cambridge University Press, Cambridge, UK.

Vukovich, F.M., 1988. Loop Current boundary variations. J. Geophys. Res. Oceans 93, 15585–15591. https://doi.org/10.1029/JC093iC12p15585.

Vukovich, F.M., 2007. Climatology of ocean features in the Gulf of Mexico using satellite remote sensing data. J. Phys. Oceanogr. 37 (3), 689–707. https://doi.org/10.1175/JPO2989.1.

Wang, Q., Pierini, S., 2020. On the role of the Kuroshio Extension bimodality in modulating the surface eddy kinetic energy seasonal variability. Geophys. Res. Lett. 47, e2019GL086308 https://doi.org/10.1029/2019GL086308.

Weisberg, R.H., Liu, Y., 2017. On the Loop current penetration into the Gulf of Mexico. J. Geophys. Res. Oceans 122, 9679–9694. https://doi.org/10.1002/2017JC013330.

Xu, F.-H., Chang, Y.-L., Oey, L.-Y., Hamilton, P., 2013. Loop Current growth and eddy shedding using models and observations: analyses of the July 2011 eddy-shedding event. J. Phys. Oceanogr. 43 (5), 1015–1027. https://doi.org/10.1175/JPO-D-12-0138.1.

Xu, C., Zhai, X., Shang, X., 2016. Work done by atmospheric winds on mesoscale ocean eddies. Geophys. Res. Lett. 43 (12), 174–180. https://doi.org/10.1002/2016GL071275.

Yan, X., Kang, D., Curchitser, E.N., Pang, C., 2019. Energetics of eddy-mean flow interactions along the western boundary currents in the North Pacific. J. Phys. Oceanogr. 49 (3), 789–810. https://doi.org/10.1175/JPO-D-18-0201.1.

Yang, Y., San Liang, X., 2018. On the seasonal eddy variability in the Kuroshio Extension. J. Phys. Oceanogr. 48, 1675–1689. https://doi.org/10.1175/JPO-D-18-0058.1.

Yang, Y., San Liang, X., Qiu, B., Chen, S., 2017. On the decadal variability of the eddy kinetic energy in the Kuroshio Extension. J. Phys. Oceanogr. 47 (5), 1169–1187. https://doi.org/10.1175/JPO-D-16-0201.1.

Yang, Y., Weisberg, R.H., Liu, Y., Liang, X.S., 2020. Instabilities and multiscale interactions underlying the Loop Current eddy shedding in the Gulf of Mexico. J. Phys. Oceanogr. 50, 1289–1317. https://doi.org/10.1175/JPO-D-19-0202.1.

Yang, Y., McWilliams, J.C., Liang, X.S., Zhang, H., Weisberg, R.H., Liu, Y., Menemenlis, D., 2021. Spatial and temporal characteristics of the submesoscale energetics in the Gulf of Mexico. J. Phys. Oceanogr. 51 (2), 475–489. https://doi.org/10.1175/JPO-D-20-0247.1.

Yin, X.-Q., Oey, L.-Y., 2007. Bred-ensemble ocean forecast of Loop Current and rings. Ocean Model. 17 (4), 300–326. https://doi.org/10.1016/j.ocemod.2007.02.005.

Zhang, Y., Hu, C., Kourafalou, V.H., Liu, Y., McGillicuddy, D.J., Barnes, B.B., Hummon, J. M., 2022. Physical characteristics and evolution of a long-lasting mesoscale cyclonic eddy in the Straits of Florida. Front. Mar. Sci. 9, 779450 https://doi.org/10.3389/fmars.2022.779450.

Zhang, Y., Hu, C., Barnes, B.B., Liu, Y., Kourafalou, V.H., McGillicuddy Jr., D.J., Cannizzaro, J.P., English, D.C., Lembke, C., 2023. Bio-optical, physical, and chemical properties of a Loop current eddy in the Gulf of Mexico. J. Geophys. Res. Oceans 128, e2022JC018726. https://doi.org/10.1029/2022JC018726.

Zhu, Y., Qiu, B., Lin, X., Wang, F., 2018. Interannual eddy kinetic energy modulations in the Agulhas Return Current. J. Geophys. Res. Oceans 123 (9), 6449–6462. https://doi.org/10.1029/2018JC014333.

Zimmerman, R.A., Biggs, D.C., 1999. Patterns of distribution of sound-scattering zooplankton in warm- and cold-core eddies in the Gulf of Mexico, from a narrowband acoustic Doppler current profiler survey. J. Geophys. Res. Oceans 104 (C3), 5251–5262. https://doi.org/10.1029/1998JC900072.